Separation Science and Technology
Publication details, including instructions for authors and subscription information:
http://www.informaworld.com/smpp/title~content=t713708471

An Explicit Solution for Concentration Polarization for Gas Separation in a Hollow Fiber Membrane

Rama Gopal Nemmani[a]; Satyanarayana V. Suggala[b]
[a] Department of Chemical Engineering, Bapatla Engineering College, Bapatla, India [b] Department of Chemical Engineering, Jawaharlal Nehru Technological University, Anantapur, India

Online publication date: 04 March 2010

To cite this Article Nemmani, Rama Gopal and Suggala, Satyanarayana V.(2010) 'An Explicit Solution for Concentration Polarization for Gas Separation in a Hollow Fiber Membrane', Separation Science and Technology, 45: 5, 581 — 591
To link to this Article: DOI: 10.1080/01496390903563074
URL: http://dx.doi.org/10.1080/01496390903563074

Separation Science and Technology, 45: 581–591, 2010

ISSN: 0149-6395 print/1520-5754 online
DOI: 10.1080/01496390903563074

Taylor & Francis
Taylor & Francis Group

An Explicit Solution for Concentration Polarization for Gas Separation in a Hollow Fiber Membrane

Rama Gopal Nemmani[1] and Satyanarayana V. Suggala[2]
[1]*Department of Chemical Engineering, Bapatla Engineering College, Bapatla, India*
[2]*Department of Chemical Engineering, Jawaharlal Nehru Technological University, Anantapur, India*

In the present work, a one-dimensional mathematical model is developed to analyze the concentration polarization phenomenon for the separation of gas mixtures in composite hollow fiber membranes. An analytical expression is developed for determining the interfacial concentration at the interface of dense and porous support layers. Further, the model accounts for the non-ideality of the gas mixture. Both co-current and counter-current flow configurations for the separation of hydrogen from a three-component mixture are studied. The effects of feed side pressure and velocity as well as permeability on concentration polarization are probed. It is apparent from this study that the concentration polarization phenomenon significantly affects the separation efficiency at higher permeability values.

Keywords binary mixture; concentration polarization; gas separation; hollow fiber module; modeling; multicomponent mixture; simulation

INTRODUCTION

Gas separation is a membrane based operation in which a feed mixture is brought in contact with a dense selective membrane at high pressure and lower pressure is applied on the other side to maintain the driving force. One of the components of gas mixture is enriched in the permeate gas that is preferentially transported through the membrane and collected on the downstream side due to the difference in its solubility and diffusivity.

When a feed mixture is brought in contact with a semi-permeable membrane, the more permeating component depletes at the membrane interface while the less permeating component accumulates. Hence a concentration gradient is set up in the fluid on the feed side and a boundary layer is formed. The phenomenon of feed side boundary layer formation due to semi-permeability of the membrane is known as concentration polarization. Hence the driving force across the membrane decreases for the more permeating component and increases for the less permeating component, thereby decreasing the selectivity of separation.

Generally it is believed that in case of gas separation and pervaporation processes, the effect of concentration polarization is low or insignificant, as the flux across the membrane is low. The invention of new membrane materials with higher permeation rates (1–3) as well as selectivities (4) has drawn the attention of many (5–10) to reconsider the effect of concentration polarization on membrane performance in gas separation. It was reported that for permeation rates greater than 1000 GPU and for selectivity above 2.0, the concentration polarization effect is significant in gas separation process (5). Further, a mathematical model was developed for analyzing the concentration polarization phenomenon (6). The phenomenon was studied in terms of ratio of fluxes with polarization to that of without polarization for both more and less permeating components. The study results indicate that the phenomenon of concentration polarization is important for industrial gas separation when the permeation rate of more permeable gas is higher than 100 GPU. A generalized correlation (7) was proposed to analyze concentration polarization in terms of a modified Peclet number for gas separation. A two-layer resistance model was developed for transport of gas mixtures through selective layer (8), which was based on free volume theory. A resistance in series model (9) incorporating boundary layer effect was also used to study the phenomenon of concentration polarization in composite hollow fiber membrane. The influence of operating variables (feed flow rate, feed pressure, permeate pressure) and membranes characteristics (permeance, selectivity) on concentration polarization was studied. The phenomenon of concentration polarization was studied under the combined influence of boundary layer and porous support layers in a composite hollow fiber membrane by developing a one-dimensional mathematical model (10). The authors concluded that the phenomenon of concentration polarization was significant in gas separation processes when permeance and the selectivity values are greater than 1000 GPU and 100, respectively.

Received 31 May 2009; accepted 6 December 2009.
Address correspondence to Satyanarayana V. Suggala, Department of Chemical Engineering, Jawaharlal Nehru Technological University, Anantapur, India. Tel.: 91-9849509167; Fax: 91-8554-272098. E-mail: svsatya7@gmail.com

In the present work, a new one-dimensional mathematical model is developed for the gas separation in a composite hollow fiber membrane. The present model differs from all previous models in that an analytical solution is developed for the estimation of species concentration at the interphase of dense and porous support layers. Further, explicit analytical solutions are developed for obtaining concentration, flux, and pressure profiles for multi-component gas mixtures. Additionally, the developed model gives a finite solution for interfacial concentration although the boundary layer thickness is equal to the inside radius of hollow fiber.

MATHEMATICAL MODEL

The transport of a gaseous component through a composite membrane may consist of the following steps, which are depicted in Fig. 1.

I. Diffusion of components from bulk feed solution to membrane surface
II. Transport though the porous layer
III. Sorption into the dense membrane at feed membrane interface
IV. Diffusion through the dense layer
V. Desorption from the dense layer on permeate side
VI. Diffusion through the permeate boundary layer

In the present study, except step VI, all other steps are taken into consideration. It is assumed that the feed is on the bore side and operation is taking place isothermally. Further, the flow in the pores of the porous support is assumed to be viscous. The concentration polarization of more permeating component A (CP_A) may be defined as:

$$CP_A = \frac{x_{A3}}{x_{A1}} \tag{1}$$

where x_{A3} and x_{A1} are the interfacial and bulk concentrations of species A. Similar equation may also be written for other component. The overall degree of polarization is defined as ratio of concentration polarization of a more permeating component to that of a less permeating component. As mentioned above, the main objective of this study is to obtain an explicit solution for interfacial concentration, x_{A3}.

The species balance on the feed side yields the following mass balance equation.

$$\frac{d(rN_A)}{dr} = 0 \tag{2a}$$

$$(rN_A)|_r = (rN_A)|_{r_2} \tag{2b}$$

where r_2 is the radius up to the interface of porous support and the selective layers. It is assumed that the transport through the dense layer takes place by the solution-diffusion mechanism and the sorption and desorption at the interfaces are fast compared to the diffusion through the membrane. Further, it is assumed that the species are in equilibrium with the selective layer on both the feed and the permeate sides. Therefore, the flux N_A through the selective membrane for more permeable component A in binary mixture may be written as:

$$N_A|_{r=r_2} = Q_A\left(x_{A3}\hat{\phi}_A P_3 - y_{A1}P_4\right) \tag{3a}$$

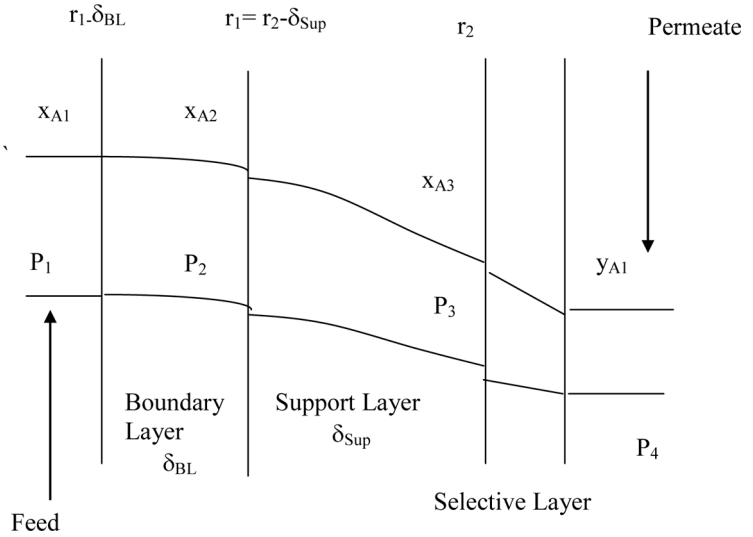

FIG. 1. Schematic diagram of resistances in a hollow fiber.

Similarly

$$N_B|_{r=r_2} = Q_B\left(x_{B3}\hat{\phi}_B P_3 - y_{B1}P_4\right) \tag{3b}$$

where $\hat{\phi}$ are permeability and fugacity coefficient, respectively.

Therefore it follows from the Eqs. (2) and (3) that

$$N_A|_r = Q_A\left(x_{A3}\hat{\phi}_A P_3 - y_{A1}P_4\right)\frac{r_2}{r} \quad \text{for} \quad r_1 \le r \le r_2 \tag{4a}$$

$$N_B|_r = Q_B\left(x_{B3}\hat{\phi}_B P_3 - y_{B1}P_4\right)\frac{r_2}{r} \quad \text{for} \quad r_1 \le r \le r_2 \tag{4b}$$

The flux variation across the support layer is small and as a consequence, the pressure drop is also small. Therefore, the total flux through the porous support is given by (10)

$$(N_A+N_B)|_r = \frac{\varepsilon r_p^2}{16\eta_m RT\tau}\frac{P_1}{r\ln\left(\frac{r_2}{r_2-\delta_{\text{sup}}}\right)}(P_1-P_3) \quad \text{for} \quad r_1 \le r \le r_2 \tag{5}$$

where η_m is the gas mixture viscosity and δ_{sup} is the thickness of the support layer. The analytical expression for pressure at the support and selective layers interface, P_3, can be obtained as follows by simultaneously solving Eqs. (4a) and (4b) with the above equation.

$$P_3 = \frac{FP_1^2 + Q_A y_{A1}P_4 + Q_B y_{B1}P_4}{FP_1 + Q_A\hat{\phi}_A x_{A3} + Q_B\hat{\phi}_B x_{B3}} \tag{6}$$

where F is defined as:

$$\mathrm{F} = \frac{\varepsilon r_p^2}{16\eta_m RT\tau}\frac{1}{r_2\ln\left(\frac{r_2}{r_2-\delta_{\text{sup}}}\right)} \tag{7}$$

Substituting Eq. (6) in Eq. (4) yields the fluxes:

$$N_A|_r = Q_A\frac{FP_1(x_{A3}P_1 - y_{A1}P_4) + Q_B P_4(x_{A3}-y_{A1})}{FP_1 + Q_A\hat{\phi}_A x_{A3} + Q_B\hat{\phi}_B x_{B3}}\frac{r_2}{r} \quad \text{for} \quad r_1 \le r \le r_2 \tag{8}$$

Similar equation may also be written for component B. The flux balance in the feed boundary layer can also be written as:

$$N_A = x_A(N_A+N_B) - cD_{AB}\frac{dx_A}{dr} \tag{9a}$$

Also, it is known that

$$x_A|_{r=r_1-\delta_{BL}} = x_{A1} \quad \text{and} \quad X_A|_{r=r_2} = x_{A3} \tag{9b}$$

where δ_{BL} is the boundary layer thickness, estimated from the following relation.

$$\delta_{BL} = \frac{D_{AB}}{k_m} \tag{10}$$

The mass transfer coefficient, k_m for laminar zone is estimated by using the following correlation (11)

$$Sh = 1.62\left(\mathrm{Re}\,Sc\frac{2r_1}{L}\right)^{0.33} \tag{11}$$

Analytical expression for x_A is obtained by solving Eq. (9a) and the details of derivation are given in Appendix 1:

$$x_4 = C_1 r^{(N_A+N_B)|_{r=r_2}\frac{r_2}{cD_{AB}}} + \left[\frac{N_A}{N_A+N_B}\right]_{r=r_2} \quad \text{for} \quad r_1-\delta_{\text{BL}} \le r \le r_2 \tag{12}$$

The general analytical equation for the boundary layer can be obtained by applying the boundary conditions Eq. (9b) for Eq. (12)

$$\frac{x_{A1} - \left[\frac{N_A}{N_A+N_B}\right]_{r=r_2}}{x_{A3} - \left[\frac{N_A}{N_A+N_B}\right]_{r=r_2}} = \left(1-\frac{\delta_{BL}}{r_2}\right)^{(N_A+N_B)|_{r=r_2}\frac{r_2}{cD_{AB}}} \tag{13}$$

Equation (13) may be further simplified for the following two cases: When the boundary layer thickness is comparable with fiber radius r_2, $\left.\frac{N_A}{N_A+N_B}\right|_{r=r_2} = x_{A1}$, suggesting that there is no separation. At this limit, for ideal gas mixtures, x_{A3} is:

$$x_{A3} = \frac{x_{A1}Q_B P_3 + (1-x_{A1})Q_A y_{A1}P_4 - x_{A1}Q_B(1-y_{A1})P_4}{Q_A(1-x_{A1})P_3 + Q_B x_{A1}P_3} \tag{14}$$

Further, if selectivity is high Q_B is negligible compared to Q_A then it follows from the above result

$$x_{A3} = \frac{y_{A1}P_4}{P_3} \tag{15}$$

When the boundary layer thickness is small, $\left|\frac{\delta_{BL}}{r_1}\right| << 1$, x_{A3} is given by one of the roots of the following quadratic equation:

$$fx_{A3}^2 + gx_{A3} + h = 0 \tag{16a}$$

where f, g, and h are:

$$f = (Q_A - Q_B)(1 - k'FP_1^2) \tag{16b}$$

$$g = [(Q_A - Q_B)(k'FP_1(P_1 + y_{A1}P_3) - x_{A1}) + k'Q_BP_3(FP_1 + Q_A) + (FP_1 + Q_B)] \quad (16c)$$

$$h = -(FP_1 + Q_B)[x_{A1} + k'Q_Ay_{A1}P_3] \quad (16d)$$

and

$$k' = \frac{\delta_{BL}}{cD_{AB}} \quad (17)$$

The details of the derivation are given in Appendix 2. In the above derivation it is assumed that the diffusivity of component in porous support layer is same as that in the boundary layer. However, it is done for two purposes. The first purpose is to illustrate the procedure of deriving the explicit quadratic equation model. The second purpose is to solve the same model for the estimation of retentate and permeate concentrations without polarization effect (i.e., $x_{A3} = x_{A1}$). In a realistic situation, the diffusivity value in the support layer is different from that in the boundary layer. The following section explains the derivation of an expression for the estimation of interfacial concentration by considering different diffusivity values in the boundary layer and support layers.

The flux balance equation for boundary layer is

$$N_A = x_A(N_A + N_B) - cD_{AB}\frac{dx_A}{dr} \quad \text{for} \quad r_1 - \delta_{BL} \le r \le r_1 \quad (18)$$

Similar equation may also be written for support layer by neglecting Knudsen diffusion (as the mean free paths of the species are of the order of angstrom units and the pore size is of the order of microns, and the feed stream pressure is as high as 15 atmospheres) and incorporating $\frac{\varepsilon}{\tau}D_{AB}$ instead of D_{AB} in Eq. (18)

$$N_A = x_A(N_A + N_B) - c\frac{\varepsilon}{\tau}D_{AB}\frac{dx_A}{dr} \quad \text{for} \quad r_1 \le r \le r_2 \quad (19)$$

The following equation for the boundary layer can be obtained after simplifying Eq. (13)

$$x_{A2} = x_{A1} + x_{A1}(N_A + N_B)|_{r=r2}\frac{r_2}{r_1}\frac{\delta}{cD_{AB}} - N_A|_{r=r_2}\frac{r_2}{r_1}\left[\frac{\delta}{cD_{AB}}\right] \quad (20)$$

and that for the support layer is

$$x_{A2} = x_{A3} - x_{A3}(N_A + N_B)|_{r=r2}\frac{\tau\delta_{\sup}}{c\varepsilon D_{AB}} + N_A|_{r=r_2}\left[\frac{\tau\delta_{\sup}}{c\varepsilon D_{AB}}\right] \quad (21)$$

Hence, from Eq. (20) and Eq. (21) that

$$x_{A1} + x_{A1}(N_A + N_B)|_{r=r_2}\frac{r_2}{r_1}\frac{\delta}{cD_{AB}} - N_A|_{r=r_2}\frac{r_2}{r_1}\left[\frac{\delta}{cD_{AB}}\right] - x_{A3} + x_{A3}(N_A + N_B)|_{r=r_2}\frac{\tau\delta_{\sup}}{c\varepsilon D_{AB}} - N_A|_{r=r_2}\left[\frac{\tau\delta_{\sup}}{c\varepsilon D_{AB}}\right] = 0 \quad (22)$$

After substituting Eq. (8) and Eq. (7) in Eq. (22), one can get a quadratic equation in terms of x_{A3}, which is similar to Eq. (16a). The exact expressions for the coefficients may be derived by following procedure similar to the one given in Appendix 2, which are lengthy. Therefore, one can always solve Eq. (22) or Eq. (13) by any numerical technique. Equation (22) may also be applicable for multi-component mixtures by replacing N_A+N_B with $\sum_{i=1}^{n} N_i$ and D_{AB} with $D_{i,m}$. In absence of experimental data of effective diffusivities of components in the mixture at high densities these are estimated using (12)

$$D_{i,m} = \left(\sum_{j-1}^{n}\frac{x_j}{D_{ij}}\right)^{-1} \quad \text{for } j \ne 1 \quad (23)$$

where the binary diffusivities at high pressure are estimated using Takahashi method (12). Further, the viscosity of the mixture can be estimated at high pressures using the Lucas method (13) and average absolute error is reported to be around 8 to 9% for dense gas mixtures (12)

$$\eta = \frac{ZF_PF_Q}{\xi} \quad (24)$$

where F_P and F_Q are polarity and quantum correction factors at high pressure for the mixture, ξ is a parameter of the mixture which has got the inverse of the viscosity units and Z is a dimensionless parameter of the model. As no experimental data is available in literature, the compressibility of the gas mixture is estimated from the Soave-Redlich-Kwong equation (14). The developed model is used to study hydrogen separation from the multi-component hydrocarbon mixture in hollow fiber module with both co-current and counter current configurations.

NUMERICAL SIMULATION

The hollow fiber is divided into N_p number of perfectly mixed reservoirs in axial direction (z) and any general K^{th} reservoir is shown in Fig. 2. The component and overall balance equations (for the K^{th} reservoir) for countercurrent configurations are as follows.

$$Y_{A1,k} = \frac{V_{A,k}}{V_{T,k}} \quad (25)$$

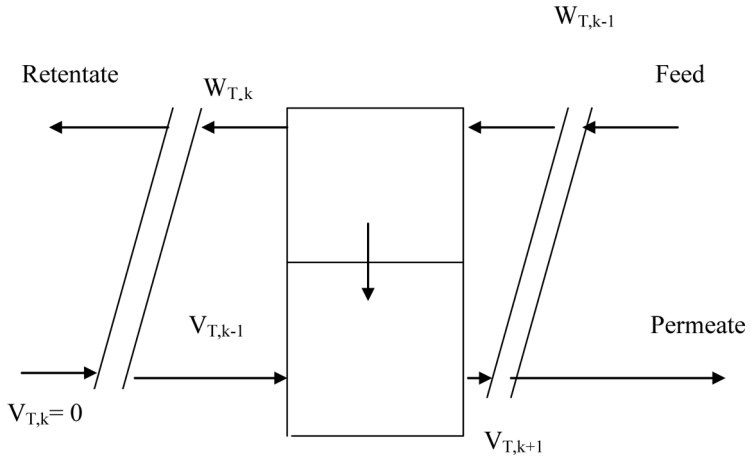

FIG. 2. Schematic diagram of Kth stage.

$$x_{A1,k} = \frac{W_{A,k}}{W_{T,k}} \tag{26}$$

$$W_{T,K+1} = W_{T,k} + \Delta A(N_A + N_B + N_c)|_{r=r_2} \tag{27}$$

$$V_{T,K} = V_{T,k-1} + \Delta A(N_A + N_B + N_c)|_{r=r_2} \tag{28}$$

$$W_{i,K+1} = W_{i,k} + \Delta A N_i|_{r=r_2} \tag{29}$$

$$V_{i,K} = V_{i,k-1} + \Delta A N_i|_{r=r_2} \tag{30}$$

$$\text{BC : for z} = 0, \text{y}_{\text{A,k}} = \left.\frac{N_A}{(N_A + N_B + N_c)}\right|_{r=r_2} \tag{31}$$

$$V_{T,1} = V_{i,1} = 0 \tag{32}$$

where i stand for any species in multi-component mixture, ΔA is the differential membrane area, and Δz is the finite length of the reservoir. For each reservoir, the retentate and permeate side mass balances (Eqs. (27)–(30)) are combined with Eq. (22) and the system of equations are solved for all the reservoirs simultaneously using "***fsolve***" routine of MATLAB software.

The separation performance is analyzed by calculating the stage cut and the enrichment factor, which are defined below:

$$\text{Stage cut} = \frac{V_{T,k=n}}{W_{T,f}} \tag{33}$$

$$\text{E}_\text{A}, \text{re} = \frac{x_{A1,re}}{x_{A1,f}} \tag{34}$$

$$\text{E}_\text{A}, \text{pe} = \frac{y_{A1,pe}}{x_{A1,f}} \tag{35}$$

Enrichment coefficient of component

$$\text{Enrichment coefficient of component } A = \frac{E_A}{E_A^0} \tag{36}$$

where $\text{E}_{\text{A,re}}$ and $\text{E}_{\text{A,pe}}$ are retentate and permeate enrichment factors for component A. The superscript '0' indicates without polarization situation.

RESULTS AND DISCUSSION

The developed model is validated for binary mixture of air (i.e., oxygen and nitrogen) by using the available data from previous study (10) and a good matching is observed (Fig. 3). Further, no experimental data is available in literature for model validation. Notably, the new model, unlike earlier model (10), does not require the equations for namely x_{A2} (boundary layer Eq. (1)) and interfacial pressure P_3 (flux through porous support: Eq. (5)). Thus the newly developed model reduces the dimensionality of the problem. The advantage is especially significant in case of multi-component gas separation by hollow fiber modules. Here it is noteworthy that the present model is distinguished from the previous model in the literature (10) as our model not only gives an explicit solution to the concentration polarization for binary as well as multi-component mixtures, but also incorporates non-ideal gas mixture behavior. The ratio of $\frac{\delta_{BL}}{r_1}$ should be small for the explicit model to be valid. For example its value is found to vary between 0.061 to 0.098 at a pressure of 55 atmospheres for the velocity varying between 1.2 to 0.25 m/s. In the present study, the new model is demonstrated for an important industrial problem of hydrogen separation from the hydrocarbon mixture.

Hydro-treatment is one of the common unit operations employed in refineries to reduce the levels of sulfur and carbon residue content of the feedstock by reacting with hydrogen. The gaseous effluent coming from the

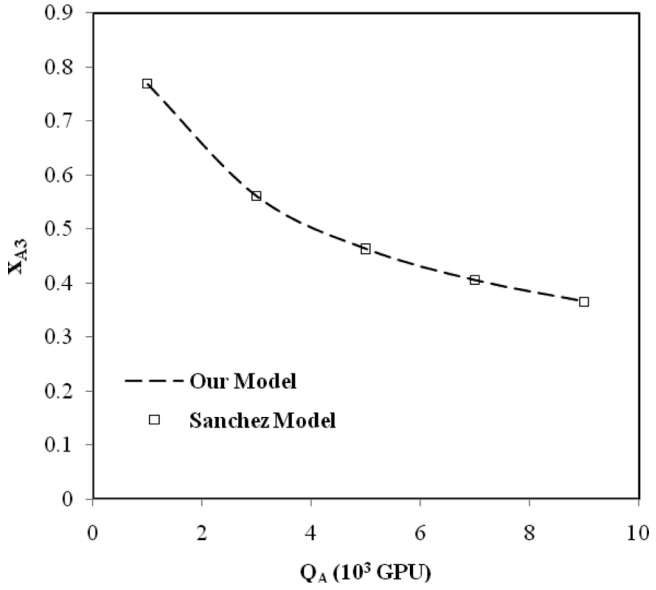

FIG. 3. Variation of interfacial concentration with Permeability ($\alpha_{AB} = 100$, u = 1.2 m/s, $P_l = 15$ atm, $P_4 = 1$ atm).

hydro-treatment contains substantial amounts of hydrogen. In order to recycle hydrogen, it must be separated from other species of the gas mixture. In general, the recycle stream is considered to be a three-component mixture of hydrogen, methane, and oxygen. Gas separation by membranes is often applied to separate hydrogen from the other gases. We have therefore used the model developed in this work to study the effect of process parameters (feed pressure, velocity) and membrane characteristics (permeability and separation factor) on the concentration polarization for hydrogen separation in a hollow fiber module with both co-current and counter-current configurations. The parameters chosen for simulation are given in Table 1. The feed gas properties are given in Table 2.

TABLE 1
Process and membrane parameters

Feed pressure (atm)	42.9–55
Permeate pressure (atm)	8
Temperature (K)	300
Permeance (GPU)	100–10000
Feed gas velocity (m/s)	0.25–1.2
Selectivity (α_{AB}, α_{AC})	100–250
Fiber OD/ID (10^{-4} m)	3/1.5
Support layer porosity	0.3
Support layer tortuosity	1.83
Support layer mean pore size (10^{-7} m)	1.5

TABLE 2
Feed gas properties and composition

	H_2 (A)	Methane (B)	Ethylene (C)
Molar fraction	0.21	0.65	0.14
Molecular weight (kg/kg · mol)	2	16	28
$D_{A,m}$ (x10^6 m^2/s)	1.776	1.47	–
Viscosity of the mixture (x 10^5 kg m^{-1} s^{-1})	4.02		

Effect of Permeation Rate

The effect of permeation rate on the concentration polarization is studied by taking permeability, Q_A values of 100 GPU and 10000 GPU. Both the retentate and the permeate sides in co-current and counter-current configurations are considered. The concentration polarization is studied in terms of stage cut versus enrichment parameter ($E_{A,\ Pe}$ or $E_{A,\ re}$) and were shown in Fig. 4. Figure 4a and Fig. 4b represent the effect of concentration polarization on co-current flow, on the retentate and the permeate sides. The corresponding plots for countercurrent configuration are shown in Figs. 4c, d.

In each graph, only two curves are presented. One for $Q_A = 100$ GPU (without polarization). The other for $Q_A = 10000$ GPU (with polarization). For $Q_A > 100$ GPU without polarization, the curves move further away from $Q_A = 10000$ GPU curve with polarization. Also for $Q_A < 10000$ GPU (with polarization) curves move closer to the curve with $Q_A = 100$ GPU without polarization. Hence the two curves are taken as base curves to represent the polarization effect for a given stage cut. Figure 4a and Fig. 4c indicate that the permeation rate curve without polarization falls below that of with polarization, suggesting that the decrease in the separation efficiency is due to polarization. Accumulation of more permeating component increases in the retentate due to increase in its polarization and decrease in driving force through the selective layer. Further, as stage cut is increasing, the gap between two curves (Fig. 4a) is also increasing till certain value and thereafter it started decreasing. Therefore, a maximum for polarization (maximum gap) is found at a particular stage cut and thereafter it is decreasing. As the stage cut increases, the transfer rates through the membrane increase, hence the polarization effect is increasing. With further increase of stage cut, almost complete removal of the more permeating component in the feed takes place. This decreases the driving force as well as the fluxes through the membrane. Ultimately, the effect of polarization decreases.

The curve of without polarization is found to lie above the curve of with polarization (Figs. 4b and d). Initially, the

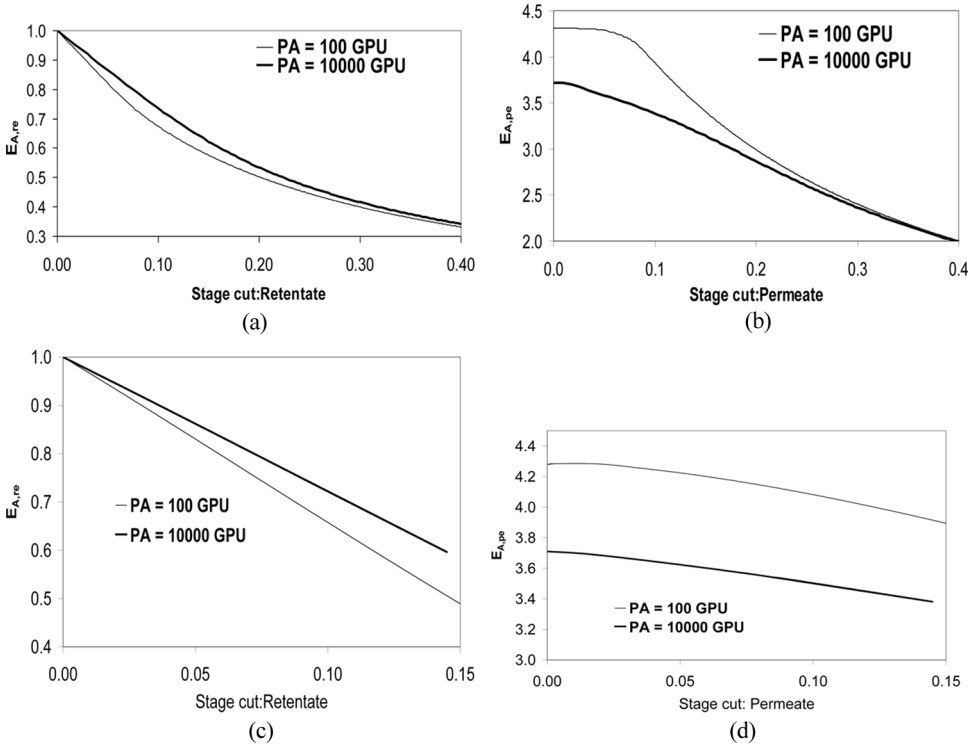

FIG. 4. Effect of concentration polarization on a co-current (a), (b) and counter-current (c), (d) configuration on the retentate and permeate sides for different permeance.

polarization effect in plots Figs. 4b, d is found to be very high owing to the high flow rates of feed at the entrance. The ratio has decreased from 4.3 to 3.7 approximately as Q_A is increased from 100 GPU to 10000 GPU. Thus the enrichment parameter is helpful in highlighting the effect of polarization on global performance of the module.

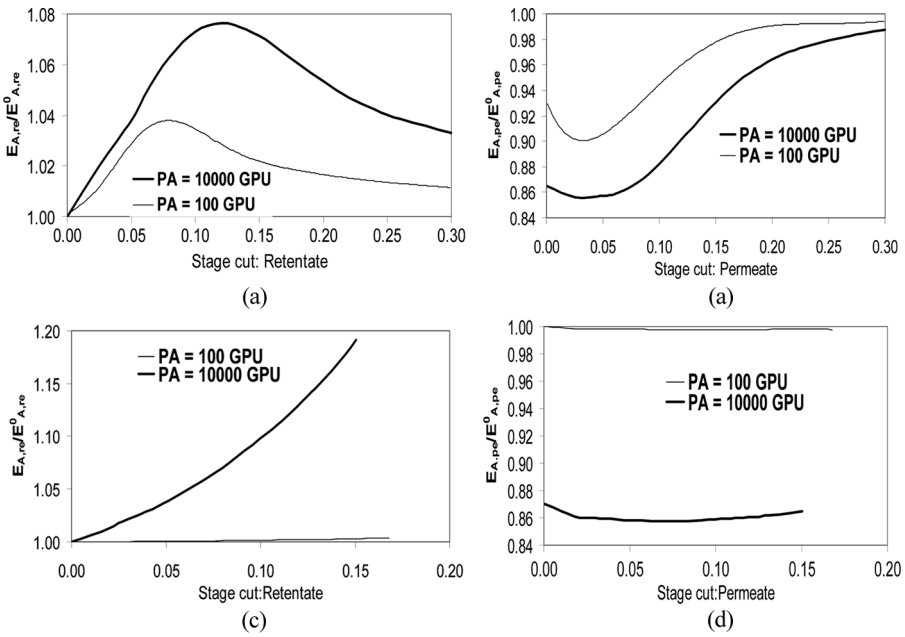

FIG. 5. Effect of concentration polarization on a co-current (a), (b) and countercurrent (c), (d) configuration for the retentate and permeate sides for different permeance value ($\alpha_{AB} = \alpha_{AC} = 100$, $P_1 = 42.9$ atm, $v = 0.77$ m/s and $P_4 = 8$ atm).

As shown in Fig. 5, the effect of the permeation rate on the concentration polarization is also studied in terms of the stage cut versus the enrichment coefficient. Fig. 5a and Fig. 5b represent the co-current plots for the retentate and the permeate sides, respectively. The corresponding plots for counter-current are presented in Fig. 5c and Fig. 5d. As the increases in stage cuts lead to increases in permeation rates through the membrane and hence the polarization effect, the curve goes through a maximum as shown in Fig. 5a. The increase in the polarization effect also increases the back diffusion of the components from the membrane interface to the bulk with concomitant decrease in the driving force. The decrease in driving force causes the fall in the enrichment coefficient.

Similarly, the same phenomenon sets up a minimum on the permeate side as shown in Fig. 5b for co-current. It is observed that the countercurrent is more adversely affected by polarization. On the retentate side, the polarization rises to about 8% for $Q_A = 10000$ GPU from 4% for $Q_A = 100$ GPU for co-current (Fig. 5a) where as the polarization effect shoots up to about 19% (for a stage cut of 0.15) for $Q_A = 10000$ GPU (Fig. 5c) from 1% for $Q_A = 100$ GPU for counter current flow. Thus these plots give the measure of influence of boundary layer and porous support layer resistances on concentration polarization.

Effect of Selectivity

Figures 6a, b represent the effect of the separation factor on concentration polarization for co-current and counter-current configurations, respectively. As the selectivity increases, the polarization also increases. In addition to this, it may be observed from Fig. 6a that the enrichment coefficient increases with increasing stage cut up to a maximum value and thereafter it decreases due to depletion of more permeating component in feed. The enrichment coefficient increases from 7.3 to 8.3% approximately as the separation factor is increased from 100 to 250 for co-current flow. Whereas, in the countercurrent configuration (Fig. 6b), the enrichment coefficient is continuously increases with increasing stage cut. The polarization increases from 13 to 19% as the separation factor increases from 100 to 250.

Effect of Feed Pressure

Feed pressure can be an important process variable with respect to the concentration polarization. The feed gas pressure is varied from 42.9 to 55 atmospheres, which is in the typical range of pressure employed in the hydro-treater. Figures 7a, b show the effect of feed pressure on the concentration polarization for co-current and counter-current configurations, respectively. As feed

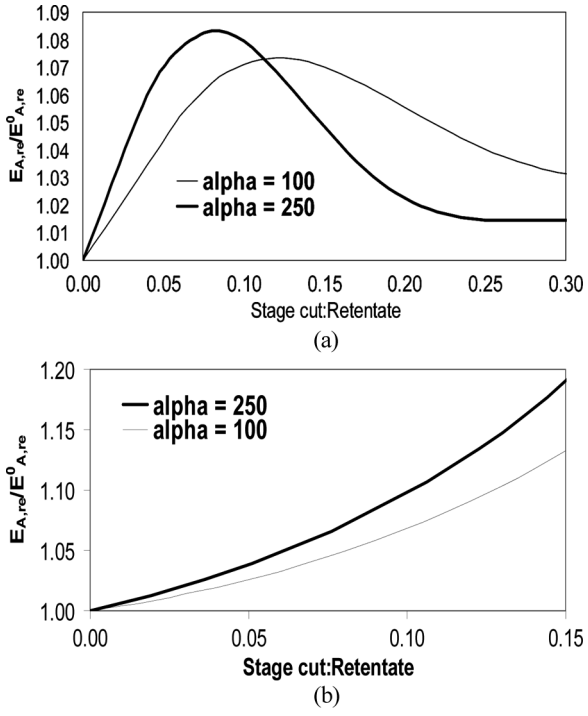

FIG. 6. Effect of concentration polarization for co-current (A) and counter current (B) configurations on the retentate side for different selectivity values. ($Q_A = 10000$ GPU, $P_1 = 42.9$ atm, $P_4 = 8$ atm, $v = 0.77$ m/s).

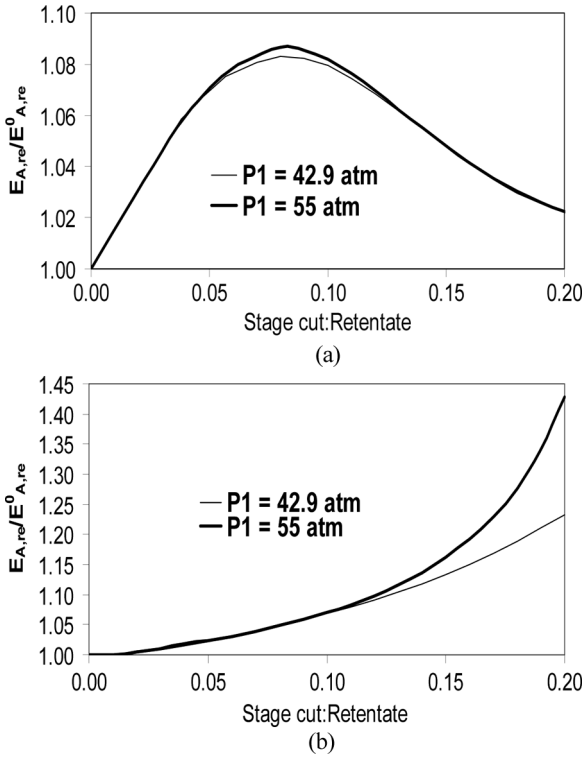

FIG. 7. Effect of concentration polarization on co-current (A) and counter current (B) configurations for different feed pressures on retentate side. ($Q_A = 10000$ GPU, $\alpha_{AB} = \alpha_{AC} = 250$, $v = 0.77$ m/s and $P_4 = 8$ atm).

pressure increases, the driving force also increases which in turn increases the polarization effect. As the feed gas pressure is increased from 42.9 to 55 atmospheres, the polarization effect has increased from 7.8 to 8.3% approximately for co-current configuration (Fig. 7a). The increase in polarization is from nearly 20% to 40% approximately for countercurrent configuration (Fig. 7b).

Effect of Feed Gas Velocity

The plots of Figs. 8a, b represent the effect of feed gas velocity on stage cut versus enrichment ratio for the retentate side in co-current and countercurrent configurations. As the feed gas velocity increases, the mass transfer coefficient also increases and the boundary layer gets thinner which leads to increases in the interfacial concentration. This decreases the degree of polarization. Clearly, the mass transfer coefficient effect is not that menacing when compared to that of other parameters studied in this work. As the stage cut increases, the effect of concentration polarization also increases in countercurrent configuration (Fig. 8b).

The enrichment coefficient increases with increasing stage cut up to 0.1. Thereafter, it decreases due to depletion of more permeating component in feed for co-current configuration (Fig. 8a). Even though, the multistage counter-current configuration is more efficient than the co-current configuration, it is more vulnerable to concentration polarization. It is therefore highly important to consider concentration polarization more seriously for the design of counter-current hollow fiber membrane modules.

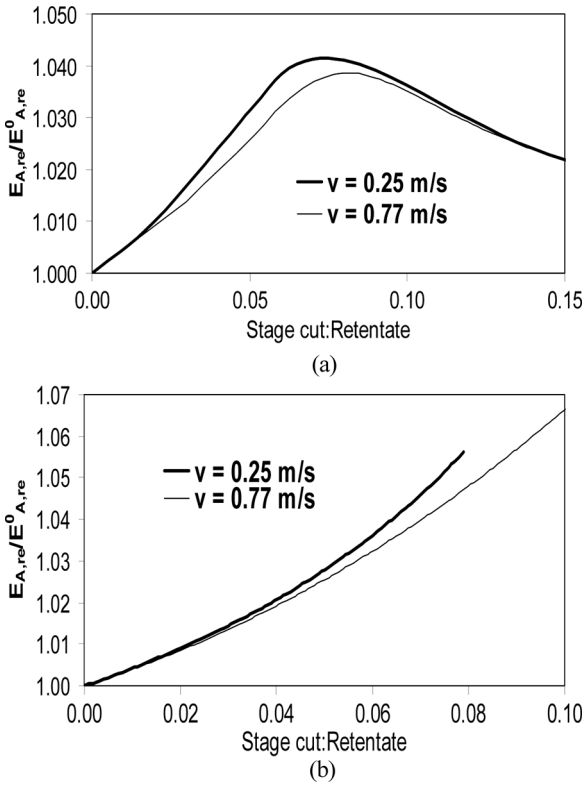

FIG. 8. Effect of concentration polarization for co-current (A) and counter current (B) configurations for different operating velocities of feed on retentate side. ($Q_A = 100$ GPU, $\alpha_{AB} = \alpha_{AC} = 250$, $P_1 = 42.9$ atm, $P_4 = 8$ atm).

CONCLUSIONS

In the present study, a mathematical model is developed that gives explicit solution for concentration polarization in the form of a quadratic equation for gas separation in a hollow fiber module with feed gas mixture taken on bore side. The usefulness of the new model is successfully demonstrated for ternary mixture separation. It is observed that the concentration polarization increases with increasing permeation rate, selectivity, and feed pressure and decreases with increasing feed velocity. The concentration polarization is more significant in counter-current configuration than in co-current configuration.

NOMENCLATURE

A	membrane area (m^2);
C_1	constant in Eq. (12)
c	Total molar concentration ($k\,mol\,m^{-3}$)
D	binary diffusivity ($m^2 s^{-1}$)
d	diameter of the fiber (m)
E	enrichment
F	parameter defined in Eq. (7)
F	parameter in Eq. (24)
f	coefficients of Eq. (16a)
g	coefficients of Eq. (16a)
h	coefficients of Eq. (16a)
J	convective flux ($k\,mol\,m^{-2}\,s^{-1}$)
k′	factor defined in Eq. (17)
k_m	mass transfer coefficient ($m\,s^{-1}$)
L	fiber length (m)
M	molecular weight (kg/kmol)
N	molar flux ($k\,mol\,m^{-2}\,s^{-1}$)
n	number of moles
n	number of reservoirs
P	pressure ($kg\,m^{-1}\,s^{-2}$)
Q	permeance (GPU $= 1 \times 10^{-6}\,cm^3$(STP)$\,cm^{-2}\,s^{-1}\,cm\,Hg^{-1}$)
R	universal gas constant ($8314\,m^3\,Pa\,kmol^{-1}\,K^{-1}$)
Re	Reynolds number
r	radius (m)
r_p	mean pore radius (m)
Sc	Schmidt number
Sh	Sherwood number
T	absolute temperature (K)
V	permeate molar rate ($kmol\,s^{-1}$)

v	velocity ($m\,s^{-1}$)
W	retentate molar rate ($kmol\,s^{-1}$)
x	mole fraction on feed side
y	mole fraction on permeate side
Z	compressibility factor
z	axial coordinate (m)

Greek Symbols

α	separation factor ($\alpha_{AB} = Q_A/Q_B$, $\alpha_{AC} = Q_A/Q_C$)
δ	boundary layer thickness (m)
ε	porosity of sub layer
η	viscosity of the mixture ($kg\,m^{-1}\,s^{-1}$)
$\hat{\phi}$	fugacity coefficient in a mixture
Δ	differential
τ	tortuosity factor
ξ	parameter in Eq. (24)

Subscripts

1	bulk.
2	membrane feed interface.
3	selective and support layer interface.
4	permeate side
A	more/most permeating component
B	less/lesser permeating Component
C	least permeating component
f	feed
i	component A, B,...
Pe	permeate
Re	retentate
sup	support layer
BL	boundary layer
m	mixture
P	polarity correction
Q	quantum correction
r	radial coordinate

Superscript

0	without concentration polarization case

REFERENCES

1. Sea, B.K.; Kusakabe, K.; Morooka, S. (1997) Pore size control and gas permeation kinetics of silica membranes by pyrolysis of phenyl-substituted ethoxysilanes with cross-flow through a porous support wall. *J. Membr. Sci.*, 130 (1): 41–52.
2. Chem, Y.T.; Wu, B.S. (1997) Preparation of composite membranes with polyimide and poly (amide-imide) skin via interfacial condensation for air separation. *J. Appl. Poly. Sci.*, 63 (6): 693–701.
3. Li, X.G.; Huang, M.R. (1996) Water-casting ultra thin-film composite membranes for air separation. *Sep. Sci. Technol.*, 3 (5): 579–603.
4. Pan, X.L.; Stroh, N.; Brunner, H.; Xiong, G.X.; Sheng, S.S. (2003) Pd/ceramic hollow-fibers for H_2 separation. *Sep. Pur. Technol.*, 32 (1–3): 265–270.
5. Haraya, K.; Hakuta, T.; Yoshitome, H. (1987) A study of concentration polarization phenomenon on the surface of gas separation membrane. *Sep. Sci. Technol.*, 22 (5): 1425–1438.
6. He, G.; Mi, Y.; Yue, L.; Chen, G. (1993) Theoretical study on concentration polarization in gas separation membrane processes. *J. Membr. Sci.*, 153 (2): 243–258.
7. Bhattacharya, S.; Hwang, S.T. (1997) Concentration polarization, separation factor, and Peclet number in membrane processes. *J. Membr. Sci.*, 132 (1): 73–90.
8. Ludtke, O.; Behling, R.D. (1998) Polarization of concentration in gas permeation. *J. Membr. Sci.*, 146 (2): 145–157.
9. Peng, F.; Liu, J.; Li, J. (2003) Analysis of the gas transport performance through PDMS/PS composite membranes using the resistances in series model. *J. Membr. Sci.*, 222 (1–2): 225–234.
10. Mourgues, A.; Sanchez, J. (2005) Theoretical analysis of concentration polarization in membrane modules for gas separation with feed inside the hollow fibers. *J. Membr. Sci.*, 252 (1–2): 133–144.
11. Cussler, E.L. (1989) *Diffusion*; Cambridge University Press: New York.
12. Reid, R.C.; Prausnitz, J.M.; Poling, B.E. (1988) *The properties of gases and liquids*, 4th Ed.; Mc Graw-Hill: New York.
13. Lucas, K. (1980) Phase Equilibria and Fluid Properties in the Chemical Industry, Dechema, Frankfurt, 573.
14. Smith, J.M.; Van Ness, H.C.; Abbott, M.M. (2003) *Introduction to chemical engineering thermodynamics*, 6th Ed.; Tata McGraw Hill.

APPENDIX 1

Multiplying on both sides of the Eq. (9a) with

$$\exp\left[-(N_A+N_B)\big|_{r=r_2}\left(\frac{r_2}{cD_{AB}}\right)\ln(r)\right]$$

we get

$$\frac{d\left(x_A\exp\left[-(N_A+N_B)\big|_{r=r_2}\left(\frac{r_2}{cD_{AB}}\right)\ln(r)\right]\right)}{dr} = -N_A\big|_{r=r_2}\left[\frac{r_2}{cD_{AB}r}\right]\exp\left[-(N_A+N_B)\big|_{r=r_2}\left[\frac{r_2}{cD_{AB}}\right]\ln(r)\right] \tag{A.1.1}$$

from which it follow that

$$x_A\exp\left[-(N_A+N_B)\big|_{r=r_2}\left[\frac{r_2}{cD_{AB}}\right]\ln(r)\right] = -N_A\big|_{r=r_2}\left[\frac{r_2}{cD_{AB}}\right]\int\frac{dr}{r^{\left(1+(N_A+N_B)_{r=r_2}\left[\frac{r_2}{cD_{AB}}\right]\right)}} \tag{A.1.2}$$

upon integration and by further simplification it follows

$$\frac{x_A}{r^{(N_A+N_B)_{r=r_2}\left(\frac{r_2}{cD_{AB}}\right)}} = C + \left[\frac{N_A}{N_A+N_B}\right]\Big|_{r=r_2}\frac{1}{r^{(N_A+N_B)_{r=r_2}\left(\frac{r_2}{cD_{AB}}\right)}} \tag{A.1.3}$$

from which Eq. (12) follows

APPENDIX 2

From Eq. (8) and analogous equation for N_B it follows that

$$N_B x_{A3} - N_A N_{A3} = \frac{FP_A^2 x_{A3} x_{B3}(Q_B - Q_A) + FP_A P_3(x_{B3} y_{A1} Q_4 - x_{A3} y_{B1} Q_B) + Q_A Q_B P_3(y_{A1} x_{B3} - y_{B1} x_{A3})}{FP_1 + Q_A x_{A3} + Q_B x_{B3}} \tag{A.2.1}$$

After simplifying Eq. (13) and substituting the above relation it follows that

$$x_{A1} = x_{A3} - \frac{\delta_{B1}}{cD_{AB}} \frac{FP_A^2 x_{A3} x_{B3}(Q_B - Q_A) + FP_A P_3(x_{B3} y_{A1} Q_4 - x_{A3} y_{B1} Q_B) + Q_A Q_B P_3(y_{A1} x_{B3} - y_{B1} x_{A3})}{FP_1 + Q_A x_{A3} + Q_B x_{B3}} \tag{A.2.2}$$

Rearranging the above equation we can get the quadratic equation as

$$\begin{aligned} &x_{A3}^2(Q_A - Q_B)(1 - k' FP_A^2) + \\ &\quad x_{A3}[(Q_A - Q_B)(k' FP_A(P_A + y_{A1} P_3) - x_{A1}) + \\ &\quad k' Q_B P_3(FP_A + Q_A) + (FP_A + Q_B)] - \\ &\quad (FP_A + Q_B)[x_{A1} + k' Q_A y_{A1} P_3] = 0 \end{aligned} \tag{A.2.2}$$